

Article

Bacterial Footprints in Elastic Pillared Microstructures

Susarrey-Arce, Arturo, Hernández-Sánchez, José Federico, Marcello, Marco, Diaz-Fernandez, Yuri, Oknianska, Alina, Sorzabal-Bellido, Ioritz, Tiggelaar, Roald, Lohse, Detlef, Gardeniers, Han, Snoeijer, Jacco, Marin, Alvaro and Raval, Rasmita

Available at <http://clock.uclan.ac.uk/33618/>

Susarrey-Arce, Arturo, Hernández-Sánchez, José Federico, Marcello, Marco, Diaz-Fernandez, Yuri, Oknianska, Alina, Sorzabal-Bellido, Ioritz, Tiggelaar, Roald, Lohse, Detlef, Gardeniers, Han et al (2018) Bacterial Footprints in Elastic Pillared Microstructures. ACS Applied Bio Materials, 1 (5). pp. 1294-1300. ISSN 2576-6422

It is advisable to refer to the publisher's version if you intend to cite from the work.

<http://dx.doi.org/10.1021/acsabm.8b00176>

For more information about UCLan's research in this area go to <http://www.uclan.ac.uk/researchgroups/> and search for <name of research Group>.

For information about Research generally at UCLan please go to <http://www.uclan.ac.uk/research/>

All outputs in CLoK are protected by Intellectual Property Rights law, including Copyright law. Copyright, IPR and Moral Rights for the works on this site are retained by the individual authors and/or other copyright owners. Terms and conditions for use of this material are defined in the <http://clock.uclan.ac.uk/policies/>

1 **Bacterial Footprints in Elastic Pillared Microstructures**

2 Arturo Susarrey-Arce,^{*,†,○} José Federico Hernández-Sánchez,^{*,‡,○} Marco Marcello,[¶]
 3 Yuri Diaz-Fernandez,[†] Alina Oknianska,[§] Ioritz Sorzabal-Bellido,[†] Roald Tiggelaar,^{||} Detlef Lohse,^{⊥,○}
 4 Han Gardeniers,^{#,○} Jacco Snoeijer,^{*,⊥} Alvaro Marin,[⊥] and Rasmita Raval^{*,†}

5 [†]Open Innovation Hub for Antimicrobial Surfaces at the Surface Science Research Centre and Department of Chemistry, University
 6 of Liverpool, Oxford Street, Liverpool L69 3BX, United Kingdom

7 [‡]Division of Physical Sciences and Engineering and Clean Combustion Research Center, King Abdullah University of Science and
 8 Technology, Thuwal 23955-6900, Saudi Arabia

9 [¶]Institute of Integrative Biology, University of Liverpool, Biosciences Building, Liverpool L69 7ZB, United Kingdom

10 [§]School of Health Sciences, Liverpool Hope University, Hope Park, Liverpool L16 9JD, United Kingdom

11 ^{||}NanoLab Cleanroom, MESA+ Institute for Nanotechnology, University of Twente, P.O. Box 217, Enschede 7500AE, The
 12 Netherlands

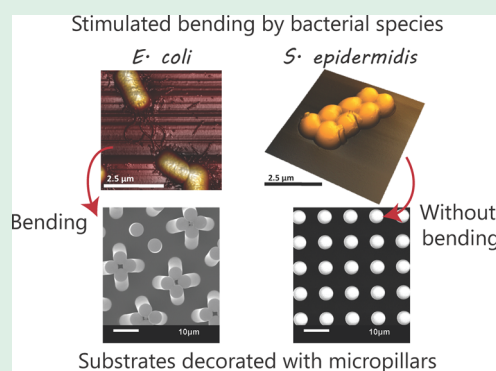
13 [⊥]Physics of Fluids Group, MESA+ Institute for Nanotechnology, J.M. Burgers Centre for Fluid Dynamics, University of Twente,
 14 P.O. Box 217, Enschede 7500AE, The Netherlands

15 [#]Mesoscale Chemical Systems, MESA+ Institute for Nanotechnology, University of Twente, P.O. Box 217, Enschede 7500AE, The
 16 Netherlands

17 **S Supporting Information**

18 **ABSTRACT:** Soft substrates decorated with micropillar arrays are known to
 19 be sensitive to deflection due to capillary action. In this work, we demonstrate
 20 that micropillared epoxy surfaces are sensitive to single drops of bacterial
 21 suspensions. The micropillars can show significant deformations upon
 22 evaporation, just as capillary action does in soft substrates. The phenomenon
 23 has been studied with five bacterial strains: *S. epidermidis*, *L. sakei*, *P.*
 24 *aeruginosa*, *E. coli*, and *B. subtilis*. The results reveal that only droplets
 25 containing motile microbes with flagella stimulate micropillar bending, which
 26 leads to significant distortions and pillar aggregations forming dimers, trimers,
 27 and higher order clusters. Such deformation is manifested in characteristic
 28 patterns that are left on the microarrayed surface following evaporation and
 29 can be easily identified even by the naked eye. Our findings could lay the
 30 ground for the design and fabrication of mechanically responsive substrates,
 31 sensitive to specific types of microorganisms.

32 **KEYWORDS:** bacteria, bending, elastic micropillars, capillarity, responsive substrates

33 **INTRODUCTION**

34 The fabrication of materials that are sensitive to physical,
 35 chemical, or biological stimuli has opened opportunities for the
 36 development of a wide variety of technological applications
 37 such as switchable adhesion, mechanosensing, and stimuli-
 38 responsive materials.^{1–6} In particular, the design of biomimetic
 39 structures,^{3,7} inspired by natural systems, has been a powerful
 40 tool in the implementation of smart, artificial systems.^{8,9} In this
 41 respect, the use of topographic surfaces is particularly
 42 interesting, with natural systems utilizing physical structures,
 43 from the nano- to the macroscale, to deliver functions such as
 44 superhydrophobicity, adhesion, and antibiofouling as demon-
 45 strated by the lotus leaf, shark skin, and gecko feet.^{4,7,9–13}

46 There has been particular interest in developing mechan-
 47 ically responsive systems.^{8,14} An excellent example is the
 48 mechanical response of micropillar arrays upon drying of water

(or water-based solutions).^{15–26} When water droplets
 49 evaporate on relatively soft elastic microstructured surfaces,
 50 capillary action can generate a significant force that is able to
 51 bend the soft micropillars. Depending on the geometry of the
 52 arrays, the capillary and elastic forces can form different pillar
 53 assemblies.^{15,16} The complexity of the assemblies varies with
 54 the pillar height and the interpillar distance. For example, large
 55 periodic chiral aggregates can be formed when the micropillars
 56 are higher and closer to each other. Each cluster of aggregates
 57 has a different potential to store elastic energy, embody
 58 information, enhance adhesion, or capture particles.^{17,18} 59

Received: May 31, 2018

Accepted: October 15, 2018

Published: October 15, 2018

60 The demonstration of mechanically responsive topographic
 61 surfaces to bacterial stimuli during evaporation of small
 62 droplets is of great interest and has not been demonstrated
 63 before. Furthermore, the deflections seen in our systems are
 64 significant, leading to pillar aggregations into dimers, trimers,
 65 and higher order clusters. Recently, the formation of biofilm
 66 strings and networks between topographic pillars has been
 67 demonstrated in liquid media;²⁷ however, the mechanical
 68 response of the pillars to bacterial presence upon evaporation
 69 is not observed. Chew and coauthors have shown small
 70 deflections of macropillared surfaces in response to the
 71 differential pressure exerted by biofilm growth within a growth
 72 chamber over a 24 h period,²⁸ while Biais²⁹ and Ng³⁰ et al.
 73 have investigated the interaction of bacterial pili with pillared
 74 structures.

75 Here, we demonstrate how epoxy-made soft surfaces
 76 containing micropillar arrays interact with suspensions of
 77 different bacterial species. Our results suggest that the presence
 78 of motile bacteria with flagella drastically increases the
 79 mechanical response of the pillars, actively bending soft
 80 topographical substrates in the area contained within the
 81 contact line. In contrast, solutions containing nonmotile
 82 bacteria do not generate such responses. We attribute this to
 83 the ability of motile bacteria to interact with each other and
 84 with their topographical environment. Importantly, the
 85 response of the microarray is sensitive to the type and
 86 concentration of bacteria in the solution. These promising
 87 results could lay the foundation for the development of devices
 88 that are selectively responsive to specific microorganisms,
 89 paving the way to construct smart, fast, and cost-effective
 90 diagnostic tools.

91 ■ RESULTS AND DISCUSSION

92 One of the key parameters in the mechanical response of soft
 93 micropillar arrays is the aspect ratio of a single pillar. We
 94 investigated the effect of the pillar aspect ratio by fabricating
 95 regular patterns of cylindrical pillars with a constant diameter
 96 ($5\ \mu\text{m}$) and interspacing ($5\ \mu\text{m}$) and with variable height
 97 (from 5 to $45\ \mu\text{m}$). The patterns were created on epoxy resin
 98 using a method described before^{31–35} based on casting
 99 uncured epoxy on a negative polydimethylsiloxane (PDMS)
 100 mold, followed by curing and mechanically removing of the
 101 mold. The micropatterns were transferred efficiently, with a
 102 high degree of fidelity, as shown by scanning electron
 103 microscopy (SEM) imaging (Figure 1 and Figure S1).

104 These microstructured substrates can be susceptible to
 105 elastocapillary forces in the presence of pure liquids. Therefore,
 106 we evaluated the effect of pure water over a surface decorated
 107 with micropillars with lengths varying from 5 to $45\ \mu\text{m}$ (Figure
 108 1) during the evaporation of water droplets (Figure 1). In
 109 these experiments, the liquid filled up the space between the
 110 pillars, resulting in an almost square-shaped droplet contour.
 111 Once the droplet spreads on the substrate, the liquid contact
 112 line is blocked by the pillared structure and remains
 113 immobilized (pinned) for the rest of the drying process.³¹
 114 Figure 1b shows that after complete evaporation, there is
 115 almost no trace of the droplet, except at the droplet contour,
 116 where lines of pillars were bent by capillary action at the
 117 contact line shown in Video S1.^{18–23,31}

118 In the systems studied, the pillar lattice was kept constant
 119 (i.e., $l = d = 5\ \mu\text{m}$), but different pillar heights (h) ranging from
 120 $h = 5$ to $45\ \mu\text{m}$ were fabricated. Thus, a range of
 121 micropatterned surfaces were generated with different aspect

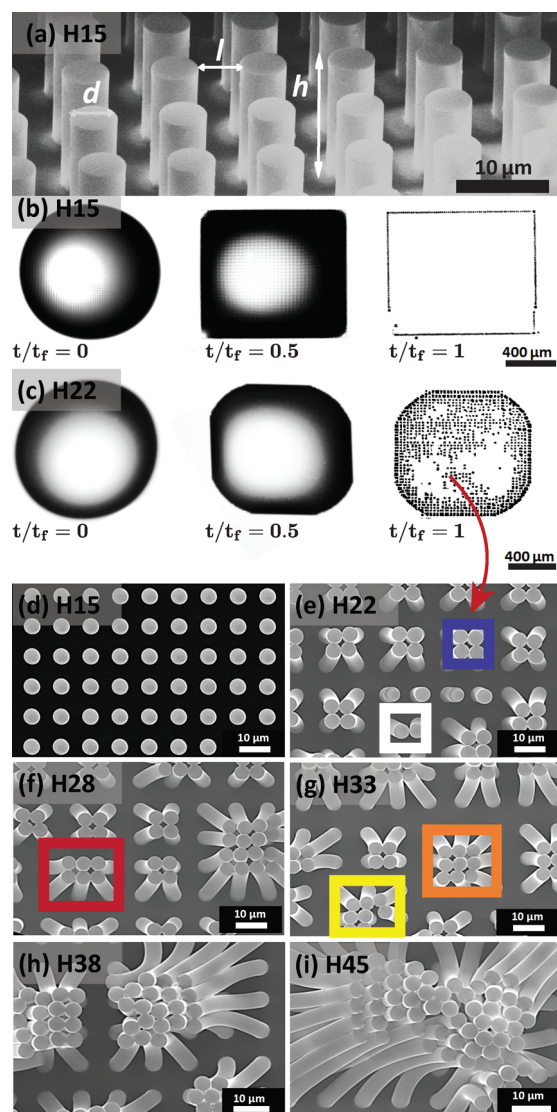


Figure 1. (a) Representative SEM image of pillared structure (H15), showing the topographic descriptors for the array. The pillars have a cylindrical shape and a height (h) of $15\ \mu\text{m}$ and a diameter (d) of $5\ \mu\text{m}$ forming a square lattice with an interpillar distance (l) = $5\ \mu\text{m}$. (b) Pure water droplet evaporating on the H15 substrate with micropillars leaving a distinct square-shaped contact line with no perturbation of pillars within this contour. (c) Pure water droplet evaporating on the H22 substrate with micropillars leaving a distinct shaped contact line pattern with significant modification of the micropillars within the contact line boundary. Time needed is represented in a dimensionless form as the ratio between the elapsed time (t) and the final evaporation time (t_f). (d–i) Pillared structures with constant ($d = 5\ \mu\text{m}$) and different pillar heights (h) of (d) $15\ \mu\text{m}$ (H15), (e) $22\ \mu\text{m}$ (H22), (f) $28\ \mu\text{m}$ (H28), (g) $33\ \mu\text{m}$ (H33), (h) $38\ \mu\text{m}$ (H38), and (i) $45\ \mu\text{m}$ (H45). SEM images are presented for the different heights after evaporation of pure water droplets, probing the sensitivity of the structures to pure elastocapillary bending.

ratios (i.e., $h/d = 3$ to $h/d = 9$). For large aspect ratio
 structures, we observed significant perturbation of the
 micropillars in the area within the contact line boundary.
 Imaging at low magnifications, or even examination by the
 naked eye, revealed that the inner part of the pattern was
 opaque, suggesting that the whole array of pillars inside the
 dried droplet perimeter was modified (Figure 1c). Higher
 magnification SEM imaging showed that this optical contrast

130 effect was caused by local bending of the micropillars (Figure
131 1d–i), with the pillars bent toward each other forming clusters
132 and adopting complex geometries, e.g., dimer (white box),
133 tetramer (blue box), hexamer (red box), octamer (yellow box),
134 and nonamer (orange box). Similar effects have been reported
135 before for larger pillar aspect ratios^{18,24,25} and were attributed
136 to the elastocapillary coalescence of the flexible structures.^{15,18}

137 In our experiments, as the aspect ratio decreased, the clusters
138 contained lower numbers of aggregated pillars until a critical
139 aspect ratio $h/d = 3$, for which no clusters were observed in the
140 inner part of the droplet (Figure 1d).

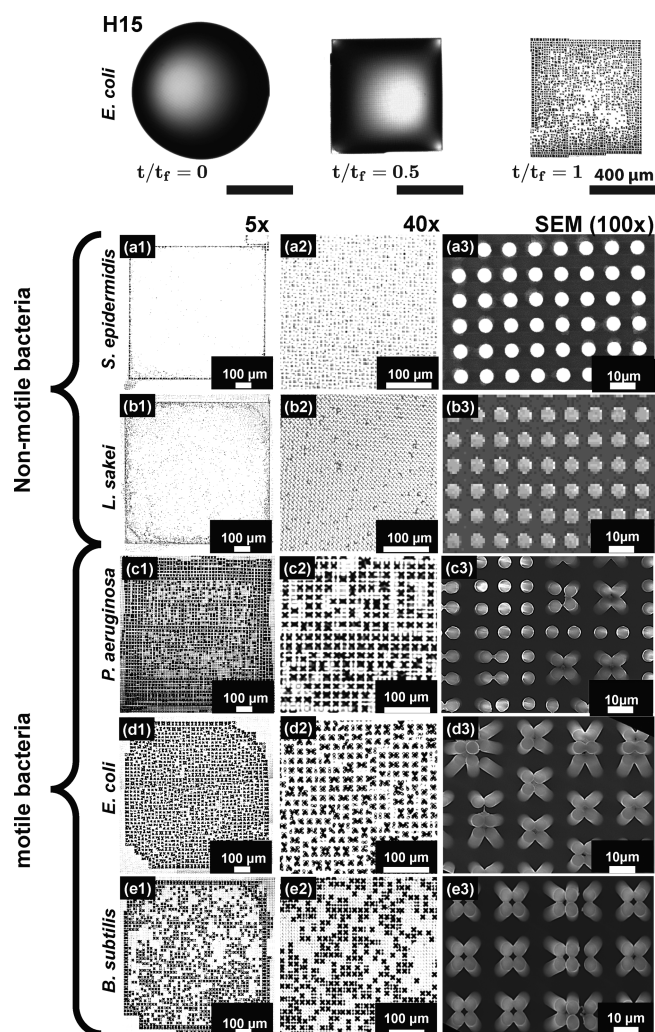
141 The deformation of the pillars, upon water evaporation, is
142 induced by the surface tension (γ) of the water/air meniscus
143 connecting the pillars, and the corresponding force scales as F_c
144 $\sim \gamma r$, where $r = d/2$ is the pillar radius.^{21,36} The natural
145 elasticity of the pillars resists deformation with an elastic force
146 $F_E \sim Elr^4/h^3$, where E is the Young modulus and l the
147 interpillar distance.¹⁸ This expression is analogous to the usual
148 beam theory for slender objects, showing that the resistance to
149 bending decreases strongly when the pillar height increases. If
150 we define the pillar bending sensitivity as the ratio of capillary
151 and elastic forces, $F_c/F_E = \gamma/El(h/r)^3$, we can conclude that it
152 is directly proportional to the cubic power of the pillar aspect
153 ratio h/r ; i.e., slender pillars are more prone to be bent by
154 surface tension, while wide pillars tend to be more stable.

155 Under our experimental conditions, no pillar coalescence is
156 observed in the area within the contact line boundary from
157 pure water when the aspect ratio is below $h/d = 3$,³¹ suggesting
158 that this is the critical aspect ratio threshold for which capillary
159 action equals restoration mechanical stress on the micropillars.
160 It is important to note that in this analysis, we are not
161 considering the effect of the contact line. This effect is
162 expected to have an enhanced deforming effect, but an
163 accurate evaluation of this factor is beyond existing
164 phenomenological modeling capabilities and will be the subject
165 of future studies. Consequently, all of the results described
166 below applies exclusively to the inner part of the dried pattern
167 left by the droplet, ignoring possible contact line effects.

168 **Bacterial-Triggered Coalescence of Pillars.** From the
169 elastocapillary assay discussed in the previous section, we
170 identified the critical region within the topographic parameter
171 space where the micropillared structure is able to resist
172 capillary deformation in the presence of pure water droplets.
173 Such a surface opens up the possibility to sense the presence of
174 a second entity introduced into water (i.e., bacterial cells),
175 which could induce a response in its own right. This critical
176 structure corresponds to an aspect ratio $h/d \approx 3$ and pillar
177 height $h = 15 \mu\text{m}$ (H15, Figure 1d), as discussed in the
178 previous section.

179 We, therefore, investigated the drying process of droplets
180 containing different bacteria species over the H15 pillared
181 structures. Similar to the case of pure water droplets, a pinned
182 square drop shape is found. However, the patterns observed
183 within the contact line formed after complete evaporation of
184 the droplets were surprisingly different for some bacteria as
185 clearly observed in Video S2.

186 Five different bacterial species, with a wide range of
187 morphological and biological characteristics were investigated:
188 *S. epidermidis*, *L. sakei*, *P. aeruginosa*, *E. coli*, and *B. subtilis*. The
189 patterns formed after evaporation of droplets containing
190 different bacteria on H15 pillar substrates (Figure 2) can be
191 classified in two main groups: one group displaying significant
192 bending of the pillars within the pattern (*P. aeruginosa*, *E. coli*,



193 **Figure 2.** Typical patterns left over H15 substrates after the
194 evaporation of different bacterial species: (a1–a3) *S. epidermidis*,
195 (b1–b3) *L. sakei*, (c1–c3) *P. aeruginosa*, (d1–d3), *E. coli*, (e1–e3) *B.*
196 *subtilis*. Here, the concentration of the different bacterial species is 10^7
197 CFU/mL. The different columns correspond to different degrees of
198 magnifications: 5 \times (left column), 40 \times (central column) by using a
199 confocal microscope, and >100 \times with SEM (right column).

200 and *B. subtilis*) and another group that does not induce any
201 responsive bending of the pillars in the center of the dried
202 patterns (*S. epidermidis* and *L. sakei*). These distinct behaviors
203 could be observed even by the naked eye in the form of a local
204 change in contrast at the surface (Figure 2, 5 \times). At higher
205 magnifications, the difference is clearly revealed to be
206 associated with the coalescence of adjacent pillars (Figure 2,
207 40 \times and SEM (100 \times)).

208 We attempted to correlate these results to the general
209 characteristics of the bacterial species used in this work (Table
210 1). Atomic force microscopy (AFM) imaging confirmed the
211 expected size and cell morphology for these bacteria: Gram-
212 negative (–) *P. aeruginosa* and *E. coli* as well as Gram-positive
213 (+) *B. subtilis* and *L. sakei* present a rod-like shape, while
214 Gram-positive (+) *S. epidermidis* has a spheroidal shape
215 (Figure S2). In addition, *L. sakei* and *S. epidermidis* are not
216 motile (no flagella present), while the other three strains have
217 flagella. From these considerations, we can conclude that the
218 different pattern types showed in Figure 2 (bending vs
219 nonbending) cannot be explained considering bacteria cell

Table 1. General Characteristics of the Different Bacterial Strains Used in the Study^a

strain	gram	shape	$L \times W_a$ (μm^2)	flagella
(a) <i>P. aeruginosa</i>	–	rod	$1.4(\pm 0.2) \times 0.8(\pm 0.2)$	yes
(b) <i>E. coli</i>	–	rod	$1.7(\pm 0.2) \times 0.9(\pm 0.2)$	yes
(c) <i>B. subtilis</i>	+	rod	$1.8(\pm 0.4) \times 0.80(\pm 0.2)$	yes
(d) <i>L. sakei</i>	+	rod	$1.5(\pm 0.4) \times 0.8(\pm 0.2)$	no
(e) <i>S. epidermidis</i>	+	spherical	$1.3(\pm 0.3) \times 1.3(\pm 0.3)$	no

^aAFM images of cells are presented in Figure S2.

213 morphology only. Similarly, the stiffness of the cell envelop
214 does not appear to play a critical role, with rigid Gram-positive
215 bacteria and softer Gram-negative bacteria distributed among
216 both pattern groups.

217 Interestingly, the different response of the microstructures
218 upon evaporation of the bacterial solutions correlates with the
219 presence or absence of flagella. Bacteria with flagella clearly
220 induce a bending response in the H15 pillars, while
221 nonflagellated bacteria are unable to bend the pillars when
222 used at the same bacterial concentration.

223 For the bacteria that induce a mechanical response, a
224 concentration dependence is observed, with deformation of
225 pillar clusters at the center of the dried droplet observed for
226 bacteria concentrations between 10^7 CFU/mL and 10^9 CFU/
227 mL, while none is observed for lower bacteria concentrations
228 (10^5 CFU/mL). At low concentrations, only the perimeter
229 near the corners of the dried square pattern presented
230 coalescence of the pillars (Figure 3a–c). This can be attributed
231 to the coffee-stain-like effect, able to drag bacterial cells toward
232 the droplet contact line, increasing the local concentration of
233 bacteria during evaporation.³¹ Interestingly, bacterial cells
234 without flagella confirm the absence of responsivity at different
235 cell concentrations (Figure 3d–f).

No clear correlation was observed between bacterial species 236
and the cluster symmetries obtained (e.g., dimer, trimer, 237
tetramer, etc.). However, the data suggests that the assemblies 238
emerge due to perturbation of the balance between capillary 239
forces and elastic restoration forces in the presence of bacteria 240
with flagella. In the next section, we discuss a possible 241
mechanism for this distinctive behavior. 242

Possible Origin of Bacteria-Induced Coalescence. In 243
the previous sections, we determined the critical pillar aspect 244
ratio, below which surface tension forces were not able to 245
induce pillar coalescence in pure water. Interestingly, the 246
responsivity is dramatically enhanced when the droplets 247
contain flagellated bacteria. While the bending process at the 248
perimeter of the contact line appears similar in both cases, 249
coalescence within the central area is triggered at smaller 250
aspect ratios by the presence of bacteria with flagella. This 251
enhanced pillar bending effect results in characteristic patterns 252
on the substrate, distinct for motile and nonmotile bacteria. 253

The possible origin of the enhanced pillar bending may be 254
related to the ability of the bacteria with flagella to adhere to 255
more than one pillar (Figure S3), thus connecting adjacent 256
pillars and inducing a mechanical deformation. In the presence 257
of bacteria with flagella, we observed, at SEM, after drying, 258
structures bridging bent pillars, while nonflagellated bacteria 259
appeared attached to single pillars. The morphology of the 260
single bacterial cells cannot be distinguished, probably due to 261
distortions on the cell envelop after evaporation, in the absence 262
of fixation. 263

These effects can also be understood by comparing the 264
length scales of bacterial structures and pillar interspacing 265
distances. The average size of the capsule for a single bacterial 266
cell is below $2 \mu\text{m}$ (Table 1), while flagella can reach tens of 267
 μm beyond the outer cell membrane.³⁷ Considering that in our 268
microstructured surfaces the interpillar distance was $5 \mu\text{m}$, 269
bacteria without flagella will predominantly fall between the 270

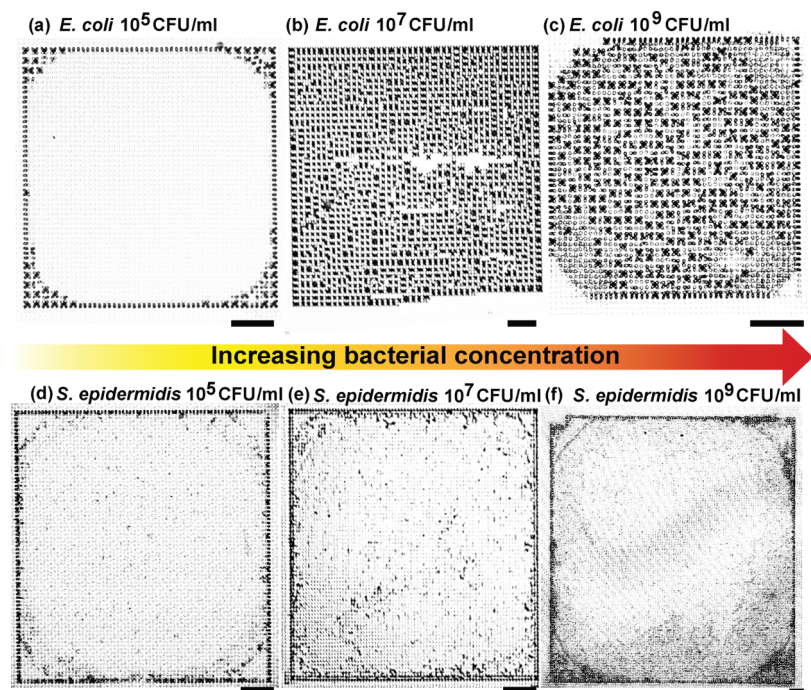
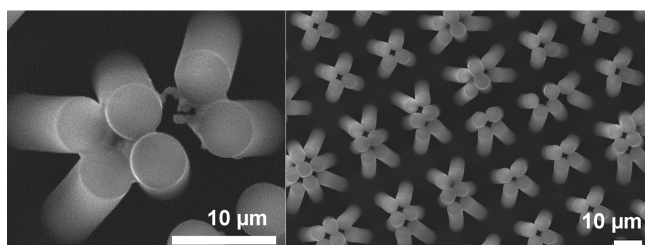


Figure 3. Effect of bacteria concentration on the bending pattern for *E. coli* and *S. epidermidis* on the H15 pillared substrate. Representative optical microscopy images for (a) 10^5 CFU/mL, (b) 10^7 CFU/mL, and (c) 10^9 CFU/mL. Scale bar in panels a–f is $100 \mu\text{m}$.

pillars or strongly adhere³⁸ to single pillars. On the other hand, bacteria with flagella,³² in which appendage sizes exceed the interpillar distance, can potentially interact with more than one pillar, leading to the observed pillar deformation. In support of this, we found evidence of bacterial matter residing between the bent pillars, after complete evaporation of droplets containing flagellated bacteria (Figure 4). Non-flagellated bacteria, on the other hand, are found attached to individual pillars only, forming nonconnecting structures (see Figures S4–S7).

B. subtilis



E. coli

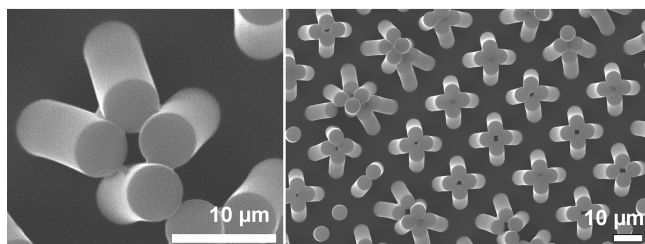


Figure 4. Representative SEM images of H15 pillared structures after drying of bacterial suspensions, showing motile bacteria (*B. subtilis* and *E. coli*) bridging the bent pillars. The concentration of the different bacterial species is 10^7 CFU/mL.

Although a more detailed investigation of bacterial behavior during the actual drying process is necessary to confirm the hypothesis proposed, our results support the potential use of pillared soft substrates to discriminate between motile and nonflagellated bacteria using a cost-effective and immediate assay based on droplet-drying, which can be performed and quickly analyzed by the naked eye. In addition, discrimination of bacterial concentration is also possible, with only samples containing concentrations above a critical threshold producing a response. We envision that by tuning the properties of the substrates, a more subtle differentiation between different microorganisms and different bacterial concentrations could be achieved in the future with this presented novel, easy to fabricate, and cost-effective technology.

CONCLUSIONS

We show that soft micropillared surfaces can be tailor-made sensitive to the presence of isolated bacterial cells in a single drop. The evaporation of water droplets and bacterial suspensions over fabricated micropillar arrays leads to very distinct micropillar deformations and patterns. Once the threshold for elastocapillary pillar coalescence is found, we observe that only bacteria with flagella can promote pillar coalescence. Such responsive micropillared surfaces could provide a platform for the development of fast and cost-effective self-responsive surfaces for bacterial detection and differentiation.

EXPERIMENTS AND METHODS

The epoxy micropillars were fabricated by casting EPO-TEK OG142-13 from Epoxy Technology into a negative replica PDMS mold, as described.^{31,32} After the resin was casted, a 1.1 mm thick glass slide was placed over the mold and placed below an ultraviolet light for 20 min until the epoxy pillar was cured. The epoxy micropillars were mechanically removed from the mold. The SEM images of the epoxy pillars are shown in Figure S1. After the sample preparation, we measured the Young modulus (E) of the bulk material and the micropillar via an axial compression test. The E value for the bulk material was 1 ± 0.3 GPa, and the E value for the H15 substrate was 0.5 ± 0.2 GPa.

Bacterial cultures were performed following recommended growing conditions for each species. *P. aeruginosa* ATCC-8626, *E. coli* ATCC-10798, and *S. epidermidis* ATCC-12228 were grown overnight at 37 °C in liquid broth medium (Oxoid Ltd., Thermo Fisher). *B. subtilis* subsp. *subtilis* ATCC-6051 and *L. sakei* DSMZ-20017 were grown overnight at 30 °C in MRS broth medium from Oxoid Ltd., Thermo Fisher. All of the cells cultures were then centrifuged and redispersed in sterile deionized water two times, finally adjusting the bacterial concentration to 10^7 colony-forming units per milliliter (CFU/mL), unless differently specified. Note that colony counting was performed after cell redispersion in deionized water to ensure cell viability.

The evaporation of all droplets was carried out placing a droplet of 5–10 $\mu\text{L} \pm 4 \mu\text{L}$ on the epoxy substrates. For droplets containing bacteria, experiments were performed in triplicates drying 5 droplets over substrates independently. The images were collected with a CMOS camera PCO Sencicam at 1 frames per second (fps). The droplet completely evaporated in approximately 2100 ± 300 s. Evaporation experiments were assessed at room temperature (21 ± 3 °C) in an atmosphere with a relative humidity of $35 \pm 5\%$.

The contact angle measurements of water and bacterial suspension droplets on epoxy surfaces were carried out by placing a water droplet with bacterial suspension of 10^7 CFU/mL on the epoxy substrates. The contact angle (CA) for H15 was $100^\circ \pm 7^\circ$, whereas the CA was $92^\circ \pm 5^\circ$ for H22, H28, and H33. For longer pillars like H38 and H45, the CA was $88^\circ \pm 3^\circ$. CA hysteresis was carried out in a similar manner as CA measurements but by tilting the substrate 45° . Experiments were performed for the H15 substrate with and without bacterial containing droplets only, the CA hysteresis was $50^\circ \pm 8^\circ$. No significant differences in CA and CA hysteresis were observed between water droplets and the deposited bacterial containing droplets. CA values are shown in Table S1.

Transmission light microscopy images of the dried patterns were collected with a Zeiss 510 confocal microscope equipped with $\times 10$, $\times 20$, and $\times 40$ air objectives. AFM measurements from the Supporting Information were obtained using a Bruker Multimode 8 and a Keysights 5500 instrument. Prior to AFM morphological analysis, a droplet of bacteria suspension (10^7 CFU/mL) was deposited onto an oxygen plasma-treated epoxy flat substrate and dried at room temperature. Estimated length (L) \times width (W_a) in Table 1 are reported within a standard deviation of 10–25% obtained by measuring 15–20 cells per bacterial strains. These tests were carried out independently in triplicates. Top-view scanning electron microscopy (SEM) imaging was performed at 20 kV. Side-view SEM was recorded after fracturing the epoxy/glass with a diamond cutter at accelerating voltages of 3 kV. Prior to SEM inspection in a JSM-6610 JEOL system, all samples were coated with 20 nm of chromium to increase the electrical conductivity. SEM images are presented without fixation, which involves several solvent exchange steps³⁹ preserving the bacterial footprints after droplet evaporation.

ASSOCIATED CONTENT

Supporting Information

The Supporting Information is available free of charge on the ACS Publications website at DOI: 10.1021/acsabm.8b00176.

SEM images of some of the pillared arrays fabricated;
AFM images of bacterial cells dried over flat epoxy

374 surfaces; close-ups of *E. coli* dried over the H15 pillared
 375 substrate; additional SEM images of bacteria on H15
 376 pillared structures; contact angle values for water and
 377 bacterial suspensions on different pillared structures
 378 (PDF)
 379 Video S1: droplet contour impalement (AVI)
 380 Video S2: pillar bending by *B. subtilis* at the latest stages
 381 of evaporation (AVI)

382 ■ AUTHOR INFORMATION

383 Corresponding Authors

384 *E-mail: A.Susarrey-Arce@liverpool.ac.uk.

385 *E-mail: Jose.HernandezSanchez@kaust.edu.sa.

386 *E-mail: j.h.snoeijer@utwente.nl.

387 *E-mail: r.raval@liverpool.ac.uk.

388 ORCID

389 Arturo Susarrey-Arce: 0000-0003-2572-223X

390 Detlef Lohse: 0000-0003-4138-2255

391 Han Gardeniers: 0000-0003-0581-2668

392 Author Contributions

393 [○]A.S.-A. and J.F.H.-S. contributed equally to this work

394 Notes

395 The authors declare no competing financial interest.

396 ■ ACKNOWLEDGMENTS

397 We would like to thank Dr. Joanna Wnietrzak and the
 398 Liverpool Centre for Cell Imaging (CCI) for help with
 399 experimental design and technical support. We also acknowl-
 400 edge the support of the Nanoinvestigation Centre at University
 401 of Liverpool (NICAL) for access to the SEM facility. Stefan
 402 Schlautmann (Mesoscale Chemical Systems, MESA+ Institute
 403 of Nanotechnology, University of Twente) is also acknowl-
 404 edged for sample fabrication. This work was partly funded by
 405 BBSRC (BB/R012415/1).

406 ■ REFERENCES

407 (1) Tawfik, S.; De Volder, M.; Copic, D.; Park, S. J.; Oliver, C. R.;
 408 Polsen, E. S.; Roberts, M. J.; Hart, A. J. Engineering of Micro-and
 409 Nanostructured Surfaces with Anisotropic Geometries and Properties.
 410 *Adv. Mater.* **2012**, *24*, 1628–1674.
 411 (2) Le, V.; Lee, J.; Chaterji, S.; Spencer, A.; Liu, Y.-L.; Kim, P.; Yeh,
 412 H.-C.; Kim, D.-H.; Baker, A. B. Syndecan-1 in Mechanosensing of
 413 Nanotopological Cues in Engineered Materials. *Biomaterials* **2018**,
 414 *155*, 13–24.
 415 (3) Chakrapani, N.; Wei, B.; Carrillo, A.; Ajayan, P. M.; Kane, R. S.
 416 Capillarity-Driven Assembly of Two-Dimensional Cellular Carbon
 417 Nanotube Foams. *Proc. Natl. Acad. Sci. U. S. A.* **2004**, *101*, 4009–
 418 4012.
 419 (4) Boesel, L. F.; Greiner, C.; Arzt, E.; Del Campo, A. Gecko-
 420 Inspired Surfaces: a Path to Strong and Reversible Dry Adhesives.
 421 *Adv. Mater.* **2010**, *22*, 2125–2137.
 422 (5) Prieto-López, L.; Williams, J. Using Microfluidics to Control Soft
 423 Adhesion. *J. Adhes. Sci. Technol.* **2016**, *30*, 1555–1573.
 424 (6) Prieto-López, L. O.; Williams, J. A. Switchable Adhesion Surfaces
 425 with Enhanced Performance Against Rough Counterfaces. *Biomimetics*
 426 **2016**, *1*, 2.
 427 (7) Kwak, M. K.; Jeong, H.-E.; Kim, T.-i.; Yoon, H.; Suh, K. Y. Bio-
 428 Inspired Slanted Polymer Nanohairs for Anisotropic Wetting and
 429 Directional Dry Adhesion. *Soft Matter* **2010**, *6*, 1849–1857.
 430 (8) Trichet, L.; Le Digabel, J.; Hawkins, R. J.; Vedula, S. R. K.;
 431 Gupta, M.; Ribault, C.; Hersen, P.; Voituriez, R.; Ladoux, B.
 432 Evidence of a Large-Scale Mechanosensing Mechanism for Cellular
 433 Adaptation to Substrate Stiffness. *Proc. Natl. Acad. Sci. U. S. A.* **2012**,
 434 *109*, 6933–6938.

(9) Liu, K.; Jiang, L. Bio-Inspired Design of Multiscale Structures for
 Function Integration. *Nano Today* **2011**, *6*, 155–175. 436
 (10) Asayesh, F.; Zarabadi, M. P.; Greener, J. A New Look at
 Bubbles During Biofilm Inoculation Reveals Pronounced Effects on
 Growth and Patterning. *Biomicrofluidics* **2017**, *11*, 064109. 437
 (11) Dean, B.; Bhushan, B. Shark-Skin surfaces for Fluid-Drag
 Reduction in Turbulent Flow: a Review. *Philos. Trans. R. Soc., A* **2010**,
 368, 4775–4806. 438
 (12) Guo, Z.; Liu, W. Biomimic from the Superhydrophobic Plant
 Leave in Nature: Binary Structure and Unitary Structure. *Plant Sci.*
2007, *172*, 1103–1112. 439
 (13) Feng, L.; Zhang, Y.; Cao, Y.; Ye, X.; Jiang, L. The Effect of
 Surface Microstructures and Surface Compositions on the Wett-
 abilities of Flower Petals. *Soft Matter* **2011**, *7*, 2977–2980. 440
 (14) Fratzl, P.; Barth, F. G. Biomaterial Systems for Mechanosensing
 and Actuation. *Nature* **2009**, *462*, 442–448. 441
 (15) Bico, J.; Roman, B.; Moulin, L.; Boudaoud, A. Adhesion:
 Elastocapillary Coalescence in Wet Hair. *Nature* **2004**, *432*, 690–690. 442
 (16) Yeh, Y.-H.; Cho, K.-H.; Chen, L.-J. Effect of Softness of
 Polydimethylsiloxane on the Hydrophobicity of Pillar-Like Patterned
 Surfaces. *Soft Matter* **2012**, *8*, 1079–1086. 443
 (17) Nill, P.; Goehring, N.; Loeffler, R.; Peschel, A.; Kern, D. P.
 Studying Bacterial Adhesion Forces: Staphylococcus Aureus on
 Elastic Poly (Dimethyl) Siloxane Substrates. *Microelectron. Eng.*
2011, *88*, 1825–1827. 444
 (18) Pokroy, B.; Kang, S. H.; Mahadevan, L.; Aizenberg, J. Self-
 Organization of a Mesoscale Bristle Into Ordered, Hierarchical
 Helical Assemblies. *Science* **2009**, *323*, 237–240. 445
 (19) Chandra, D.; Yang, S. Stability of High-Aspect-Ratio Micro-
 pillar Arrays Against Adhesive and Capillary Forces. *Acc. Chem. Res.*
2010, *43*, 1080–1091. 446
 (20) Chandra, D.; Yang, S. Capillary-Force-Induced Clustering of
 Micropillar Arrays: is it Caused by Isolated Capillary Bridges or by the
 Lateral Capillary Meniscus Interaction Force? *Langmuir* **2009**, *25*,
 10430–10434. 447
 (21) Roman, B.; Bico, J. Elasto-Capillarity: Deforming an Elastic
 Structure with a Liquid Droplet. *J. Phys.: Condens. Matter* **2010**, *22*,
 493101. 448
 (22) Marchand, A.; Weijs, J. H.; Snoeijer, J. H.; Andreotti, B. Why is
 Surface Tension a Force Parallel to the Interface? *Am. J. Phys.* **2011**,
 79, 999–1008. 449
 (23) Weijs, J. H.; Andreotti, B.; Snoeijer, J. H. Elasto-Capillarity at
 the Nanoscale: on the Coupling between Elasticity and Surface
 Energy in Soft Solids. *Soft Matter* **2013**, *9*, 8494–8503. 450
 (24) Yang, M. T.; Fu, J.; Wang, Y.-K.; Desai, R. A.; Chen, C. S.
 Assaying Stem Cell Mechanobiology on Microfabricated Elastomeric
 Substrates with Geometrically Modulated Rigidity. *Nat. Protoc.* **2011**,
 6, 187–213. 451
 (25) Wei, Z.; Schneider, T.; Kim, J.; Kim, H.-Y.; Aizenberg, J.;
 Mahadevan, L. Elastocapillary Coalescence of Plates and Pillars. *Proc.*
R. Soc. London, Ser. A **2015**, *471*, 20140593. 452
 (26) Ledesma-Aguilar, R.; Laghezza, G.; Yeomans, J. M.; Vella, D.
 Using Evaporation to Control Capillary Instabilities in Micro-
 Systems. *Soft Matter* **2017**, *13*, 8947–8956. 453
 (27) Jahed, Z.; Shahsavan, H.; Verma, M. S.; Rogowski, J. L.; Seo, B.
 B.; Zhao, B.; Tsui, T. Y.; Gu, F. X.; Mofrad, M. R. K. Bacterial
 Networks on Hydrophobic Micropillars. *ACS Nano* **2017**, *11*, 675–
 683. 454
 (28) Chew, S. C.; Kundukad, B.; Teh, W. K.; Doyle, P.; Yang, L.;
 Rice, S. A.; Kjelleberg, S. Mechanical Signatures of Microbial Biofilms
 in Micropillar-Embedded Growth Chambers. *Soft Matter* **2016**, *12*,
 5224–5232. 455
 (29) Biais, N.; Ladoux, B.; Higashi, D.; So, M.; Sheetz, M.
 Cooperative Retraction of Bundled Type IV Pili Enables Nanonewton
 Force Generation. *PLoS Biol.* **2008**, *6*, 1–7. 456
 (30) Ng, D.; Harn, T.; Altindal, T.; Kolappan, S.; Marles, J. M.; Lala,
 R.; Spielman, I.; Gao, Y.; Hauke, C. A.; Kovacicova, G.; Verjee, Z.;
 Taylor, R. K.; Biais, N.; Craig, L. The *Vibrio cholerae* Minor Pili 501

- 503 TcpB Initiates Assembly and Retraction of the Toxin-Coregulated
504 Pilus. *PLoS Pathog.* **2016**, *12*, 1–31.
- 505 (31) Susarrey-Arce, A.; Marin, A.; Massey, A.; Oknianska, A.; Díaz-
506 Fernandez, Y.; Hernández-Sánchez, J. F.; Griffiths, E.; Gardeniers, J.
507 G. E.; Snoeijer, J. H.; Lohse, D.; Raval, R. Pattern Formation by
508 Staphylococcus Epidermidis via Droplet Evaporation on Microoillars
509 Arrays at a Surface. *Langmuir* **2016**, *32*, 7159–7169.
- 510 (32) Hochbaum, A. I.; Aizenberg, J. Bacteria Pattern Spontaneously
511 on Periodic Nanostructure Arrays. *Nano Lett.* **2010**, *10*, 3717–3721.
- 512 (33) Li, X.; Cheung, G. S.; Watson, G. S.; Watson, J. A.; Lin, S.;
513 Schwarzkopf, L.; Green, D. W. The Nanotipped Hairs of Gecko Skin
514 and Biotemplated Replicas Impair and/or Kill Pathogenic Bacteria
515 with High Efficiency. *Nanoscale* **2016**, *8*, 18860–18869.
- 516 (34) Kim, P.; Epstein, A. K.; Khan, M.; Zarzar, L. D.; Lipomi, D. J.;
517 Whitesides, G. M.; Aizenberg, J. Structural Transformation by
518 Electrodeposition on Patterned Substrates (STEPS): A New Versatile
519 Nanofabrication Method. *Nano Lett.* **2012**, *12*, 527–533.
- 520 (35) Pokroy, B.; Epstein, A. K.; Persson-Gulda, M. C. M.; Aizenberg,
521 J. Fabrication of Bioinspired Actuated Nanostructures with Arbitrary
522 Geometry and Stiffness. *Adv. Mater.* **2009**, *21*, 463–469.
- 523 (36) Hadjittofis, A.; Lister, J. R.; Singh, K.; Vella, D. Evaporation
524 Effects in Elastocapillary Aggregation. *J. Fluid Mech.* **2016**, *792*, 168–
525 185.
- 526 (37) Haiko, J.; Westerlund-Wikström, B. The Role of the Bacterial
527 Flagellum in Adhesion and Virulence. *Biology* **2013**, *2*, 1242–1267.
- 528 (38) Hizal, F.; Choi, C.-H.; Busscher, H. J.; van der Mei, H. C.
529 Staphylococcal Adhesion, Detachment and Transmission on Nano-
530 pillared Si Surfaces. *ACS Appl. Mater. Interfaces* **2016**, *8*, 30430–
531 30439.
- 532 (39) Susarrey-Arce, A.; Sorzabal-Bellido, I.; Oknianska, A.; McBride,
533 F.; Beckett, A. J.; Gardeniers, J. G. E.; Raval, R.; Tiggelaar, R. M.; Diaz
534 Fernandez, Y. A. Bacterial Viability on Chemically Modified Silicon
535 Nanowire Arrays. *J. Mater. Chem. B* **2016**, *4*, 3104–3112.